This is the accepted manuscript made available via CHORUS. The article has been published as:

Robust Zero-Field Skyrmion Formation in FeGe Epitaxial Thin Films

J. C. Gallagher, K. Y. Meng, J. T. Brangham, H. L. Wang, B. D. Esser, D. W. McComb, and F. Y. Yang

Phys. Rev. Lett. **118**, 027201 — Published 9 January 2017

DOI: 10.1103/PhysRevLett.118.027201

Robust Zero-Field Skyrmion Formation in FeGe Epitaxial Thin Films

J. C. Gallagher[1], K. Y. Meng[1], J. T. Brangham[1], H. L. Wang[1], B. D. Esser[2], D. W. McComb[2], and F. Y. Yang[1]

[1]Department of Physics, The Ohio State University, Columbus, OH, 43210, USA

[2]Center for Electron Microscopy and Analysis, Department of Materials Science and Engineering, The Ohio State University, Columbus, OH, 43212, USA

Abstract

B20 phase magnetic materials have been of significant interests because they enable magnetic skyrmions. One major effort in this emerging field is the stabilization of skyrmions at room temperature and zero magnetic field. We grow phase-pure, high crystalline quality FeGe epitaxial films on Si(111). Hall effect measurements reveal strong topological Hall effect after subtracting the ordinary and anomalous Hall effects, demonstrating the formation of high density skyrmions in FeGe films between 5 and 275 K. In particular, substantial topological Hall effect was observed at zero magnetic field, showing a robust skyrmion phase without the need of an external magnetic field.

Magnetic skyrmions are topological spin textures,[1-8] which have attracted significant interests in recent years due to their intriguing magnetic interactions and attractive attributes for magnetic storage and other spintronic applications.[3,4,9] The B20 phase FeGe, MnSi, and related compounds received particular attentions because in their non-centrosymmetric B20 cubic structure, the spin-orbit coupling induced Dzyaloshinskii-Moriya interaction (DMI) enables non-collinear spin alignment and skyrmion formation.[3,10,11] The topological spin texture of skyrmions allows skyrmion motion driven by an electrical current at a very low current density.[12,13] For technological applications, it is desired to have skyrmion phase at room temperature and zero magnetic field. To date, prominent skyrmion phase in B20 materials can only be realized below room temperature and at finite magnetic fields.[1-9,12-16] A major effort in this field is to increase their magnetic ordering temperature and to stabilize the skyrmion phase at zero magnetic field. Thin films are a good avenue for achieving these goals since finite size effect can increase the range of temperatures (T) and magnetic fields (H) within which the skyrmions are stable.[4,16-18] FeGe has the highest ordering temperature of 278 K among the B20 materials.[3] Here, we report the observation of robust skyrmion formation at zero magnetic field in phase-pure FeGe epitaxial films.

FeGe epitaxial films were deposited by off-axis sputtering with a base pressure of 4×10^{-11} Torr.[19-21] Si(111) substrates were treated by HF immediately before loading into the sputter system and FeGe films were grown at a temperature of 290°C using DC sputtering with a deposition rate of 0.94 nm/minute (see Supplementary Materials for details on film growth). FeGe film thicknesses of 100, 65, and 36 nm are used for this study. All FeGe films exhibit pure B20 phase as shown in the X-ray diffraction (XRD) scans in Fig. 1. The out-of-plane lattice constants are 4.682 Å, 4.684 Å, and 4.685 Å for the 100, 65, and 36 nm FeGe films, respectively,

which closely match that of Si with a 30° rotation (5.431 Å × cos 30° = 4.703 Å) [see Supplementary Materials for more XRD results].

The 100 nm FeGe film was imaged by Scanning Transmission Electron Microscopy (STEM) using an FEI probe-corrected Titan^3 80-300 S/TEM. Figure 2(a) shows a STEM image of the FeGe/Si interface viewed along the $<110>_{FeGe}$, which clearly reveals the B20 lattice of the FeGe film and the diamond structure of the Si substrate. There is a 1.2 to 1.5 nm interfacial region due to the formation of a Fe-Ge-Si transition layer from diamond-Si to B20-FeGe. An atomic resolution STEM image in Fig. 2(b) shows two intertwined networks of parallelograms with a ~70° rotation between the two networks as illustrated in Fig. 2(c). To the best of our knowledge, this is the first clear observation of the B20 atomic ordering of FeGe by STEM, demonstrating the high crystalline quality of the FeGe epitaxial films.

Magnetic hysteresis loops of the FeGe films were measured using a Superconducting Quantum Interface Device (SQUID) magnetometer at 5 to 300 K. Figure 3(a) shows the out-of-plane hysteresis loop for the 36 nm FeGe film at 5 K. The three FeGe films were patterned into a standard Hall bar structure with a width of 0.5 mm. Longitudinal (ρ_{xx}) and Hall (ρ_{xy}) resistivity measurements were taken using a Physical Property Measurement System (PPMS). A constant current density of 2,000 A/cm^2 is applied while longitudinal and Hall voltages were measured to obtain ρ_{xx} and ρ_{xy}. Figure 3(b) shows ρ_{xy} at 5 K for the 36 nm film, where we note three features: (1) a linear background at large fields (> 2 T), (2) a magnetic reversal behavior at intermediate fields that follows the magnetization hysteresis loop, and (3) a Hall hysteresis loop within ±3000 Oe that does not follow the magnetization hysteresis loop. These three features can be attributed to the ordinary Hall effect, anomalous Hall effect, and topological Hall effect, respectively. The total Hall resistivity is a combination of these three terms:[14,15] $\rho_{xy} = R_{\mathrm{o}}H + R_{\mathrm{s}}M + \rho_{\mathrm{TH}}$, where

R_o and R_s are the ordinary and anomalous Hall coefficient, respectively, M the out-of-plane magnetization, and ρ_{TH} the topological Hall resistivity. When a current is driven through the FeGe film, the electrons experience an emergent electromagnetic field through interaction with the skyrmions.[3] Consequently, the electrons are scattered off the skyrmions in a direction opposite of the anomalous Hall effect, generating a topological Hall voltage.[5,22,23] In Fig. 3(b), the coercivity (H_c) of the Hall hysteresis loop is 2400 Oe, which is much larger than the H_c = 240 Oe for the magnetization hysteresis in Fig. 3(a); meanwhile, the Hall resistivity switches sign before reaching zero field. These are signatures of the topological Hall effect.[16]

The anomalous Hall coefficient can be modeled into a power-law function of ρ_{xx}, $R_s = b\rho_{xx}^2 + c\rho_{xx}$, where the quadratic $b\rho_{xx}^2$ term is due to a scattering independent mechanism and the linear $c\rho_{xx}$ term is caused by skew scattering.[22,24] A log-log plot of the anomalous Hall resistivity (ρ_{AH}) vs. ρ_{xx} at $|H|$ = 4 T reveals a linear dependence with a slope of 2.3, suggesting that the anomalous Hall effect is dominated by the scattering independent mechanisms and the $c\rho_{xx}$ term can be neglected[24] (see Supplementary Materials for details). In addition, all FeGe films show very small magnetoresistance (<0.7% at fields up to 7 T for all samples); thus R_s is approximately magnetic field independent. At $|H| \geq 2$ T, the FeGe films are in the saturated ferromagnetic state and the topological Hall effect is absent (ρ_{TH} = 0) due to the lack of skyrmions. As a result, the Hall resistivity can be simplified as, $\frac{\rho_{xy}}{H} = R_o + b\frac{\rho_{xx}^2 M_s}{H}$. By plotting $\frac{\rho_{xy}}{H}$ vs. $\frac{\rho_{xx}^2 M_s}{H}$ which exhibits a linear dependence, R_o and b can be obtained from the y-intercept and the slope, respectively.[14] The topological Hall resistivity was then extracted by subtracting out the ordinary and anomalous Hall resistivity, as shown in Fig. 3(c) for the three FeGe epitaxial films (see Supplementary Materials for details on background subtraction). Three notable features are observed in Fig. 3(c). First, strong topological Hall effect (ρ_{TH} = 94.8 $\pm$ 1.6 nΩ-cm

for the 36 nm film) is detected at 5 K which is significantly lower than the temperature window for skyrmion formation in bulk FeGe.[5,25] Second, all three films exhibit clear hysteresis where the switching of ρ_{TH} is opposite to those of the anomalous Hall effect and magnetization hysteresis (indicated by the arrows). Third, there are significant remanent values of ρ_{TH} at $H = 0$ for all three films, which demonstrates robust skyrmion formation at zero field. This stable skyrmion phase without the need of an applied magnetic field is desired for technological applications.

As the temperature increases, ρ_{TH} continues to increase up to 275 K, indicating the enhancement of the topological Hall effect. The topological Hall effect is very large for all three FeGe films, e.g., $\rho_{TH} = 918 \pm 5$ nΩ-cm at 250 K for the 36 nm film, which is more than five times larger than the highest values of ρ_{TH} previously reported for B20 skyrmion materials [see Fig. S7 in the Supplementary Materials].[4,13,15] The magnetic field at the maximum ρ_{TH} for the FeGe films shifts toward lower fields with decreasing thickness, indicating that skyrmion formation requires lower energy for thinner films. The lower energy costs for skyrmion formation at smaller thicknesses also result in higher overall skyrmion densities, thus larger ρ_{TH}, as shown in Fig. 3(d).

The main result of this work is the robust skyrmion formation at zero magnetic field, as can be seen from the large remanent values of ρ_{TH} in Fig. 3(c). The large remanent ρ_{TH} indicates that a significantly high skyrmion density persists at zero magnetic field. To quantitatively characterize the zero-field skyrmion stability, we define the *Squareness* of ρ_{TH}, *Squareness* $\equiv \rho_{TH}(H = 0)/\rho_{TH}(\text{max})$, and plot it as a function of temperature for the three FeGe films in Fig. 3(e). The *Squareness* is as high as 0.77 for the 100 nm film at $T = 5$ K and

decreases with increasing temperature. Substantial *Squareness* persists to high temperatures, especially for the thinner films, for example, *Squareness* = 0.39 at 150 K for the 36 nm film.

Figures 4(a)-4(f) show the field and temperature dependencies of ρ_{TH} for the 100, 65, and 36 nm films for both the decreasing and increasing field branches of the hysteresis loops, indicating that the range of the skyrmion phase and the magnitude of ρ_{TH} depend on the FeGe thickness. In bulk FeGe, the skyrmion phase is metastable, with its stable counterpart being a helical phase with a helical period of 68-70 nm.[25] Under geometric constraints, the skyrmion phase becomes more stable.[4,5,14,16] For the 100 nm film, the thickness is about 1.5 times larger than the helical period observed in bulk FeGe, while its skyrmion phase is much broader and stronger than in the bulk. For the 65 nm film, the thickness is comparable to the helical period of the bulk; the skyrmion phase is stabilized in a broader field range and becomes stronger as compared with that of the 100 nm film at low temperatures. At 36 nm, the film thickness is about half the helical period of the bulk FeGe and the skyrmion phase expands further in both the field and temperature axes. Stabilization of the skyrmion phase in epitaxial FeGe films likely arises from the epitaxy with the Si substrate and small thicknesses, which suppress the helical phase and favor skyrmion formation. Figures 4(g) and 4(h) show a zoom-in view of ρ_{TH} for the 36 nm film (-0.15 to 0.15 T) to highlight the large remanent ρ_{TH} between 5 and 275 K.

In summary, the robust skyrmion formation at zero field as revealed by the large remanent topological Hall resistivity in FeGe films demonstrates that skyrmions can be stabilized as the ground state (zero field) in epitaxial thin films. This is enabled by the deposition of pure B20 phase, high quality epitaxial FeGe thin films using off-axis UHV sputtering. The large topological Hall resistivity (up to 1067 $\pm$ 3 nΩ-cm) observed in the FeGe films is much larger

than previously reported, indicating a high density of skyrmions which can be created at a low energy cost.

Acknowledgements

This work was primarily supported by the U.S. Department of Energy (DOE), Office of Science, Basic Energy Sciences, under Grants No. DE-SC0001304 (sample growth and characterizations of structural and transport properties). This work was supported in part by the National Science Foundation under Grant No. DMR-1507274 (magnetization measurements) and Center for Emergent Materials, an NSF-funded MRSEC, under Grant No. DMR-1420451 (STEM characterization).

References:

1. S. V. Grigoriev, V. A. Dyadkin, E. V. Moskvin, D. Lamago, T. Wolf, H. Eckerlebe, and S. V. Maleyev, *Phys. Rev. B* **79**, 144417 (2009).
2. S. V. Grigoriev, V. A. Dyadkin, D. Menzel, J. Schoenes, Y. O. Chetverikov, A. I. Okorokov, H. Eckerlebe, and S. V. Maleyev, *Phys. Rev. B* **76**, 224424 (2007).
3. N. Nagaosa and Y. Tokura, *Nature Nano.* **8**, 899 (2013).
4. Y. F. Li, N. Kanazawa, X. Z. Yu, A. Tsukazaki, M. Kawasaki, M. Ichikawa, X. F. Jin, F. Kagawa, and Y. Tokura, *Phys. Rev. Lett.* **110**, 117202 (2013).
5. X. Z. Yu, N. Kanazawa, Y. Onose, K. Kimoto, W. Z. Zhang, S. Ishiwata, Y. Matsui, and Y. Tokura, *Nature Mater.* **10**, 106 (2011).
6. K. Shibata, X. Z. Yu, T. Hara, D. Morikawa, N. Kanazawa, K. Kimoto, S. Ishiwata, Y. Matsui, and Y. Tokura, *Nature Nanotech.* **8**, 723 (2013).
7. S. Seki, X. Z. Yu, S. Ishiwata, and Y. Tokura, *Science* **336**, 198 (2012).
8. N. Kanazawa, Y. Onose, T. Arima, D. Okuyama, K. Ohoyama, S. Wakimoto, K. Kakurai, S. Ishiwata, and Y. Tokura, *Phys. Rev. Lett.* **106**, 156603 (2011).
9. N. Romming, C. Hanneken, M. Menzel, J. E. Bickel, B. Wolter, K. von Bergmann, A. Kubetzka, and R. Wiesendanger, *Science* **341**, 636 (2013).
10. T. Moriya, *Phys. Rev.* **120**, 91 (1960).
11. I. Dzyaloshinsky, *J. Phys. Chem. Solids* **4**, 241 (1958).
12. T. Schulz, R. Ritz, A. Bauer, M. Halder, M. Wagner, C. Franz, C. Pfleiderer, K. Everschor, M. Garst, and A. Rosch, *Nature Phys.* **8**, 301 (2012).
13. X. Z. Yu, N. Kanazawa, W. Z. Zhang, T. Nagai, T. Hara, K. Kimoto, Y. Matsui, Y. Onose, and Y. Tokura, *Nature Comm.* **3**, 988 (2012).
14. S. X. Huang and C. L. Chien, *Phys. Rev. Lett.* **108**, 267201 (2012).
15. N. A. Porter, J. C. Gartside, and C. H. Marrows, *Phys. Rev. B* **90**, 024403 (2014).
16. N. Kanazawa, M. Kubota, A. Tsukazaki, Y. Kozuka, K. S. Takahashi, M. Kawasaki, M. Ichikawa, F. Kagawa, and Y. Tokura, *Phys. Rev. B* **91**, 041122 (2015).
17. U. K. Rossler, A. N. Bogdanov, and C. Pfleiderer, *Nature* **442**, 797 (2006).
18. A. Mehlin, F. Xue, D. Liang, H. F. Du, M. J. Stolt, S. Jin, M. L. Tian, and M. Poggio, *Nano Lett.* **15**, 4839 (2015).
19. B. Peters, A. Alfonsov, C. G. F. Blum, S. J. Hageman, P. M. Woodward, S. Wurmehl, B. Büchner, and F. Y. Yang, *Appl. Phys. Lett.* **103**, 162404 (2013).
20. A. J. Hauser, R. E. A. Williams, R. A. Ricciardo, A. Genc, M. Dixit, J. M. Lucy, P. M. Woodward, H. L. Fraser, and F. Y. Yang, *Phys. Rev. B* **83**, 014407 (2011).
21. H. L. Wang, C. H. Du, Y. Pu, R. Adur, P. C. Hammel, and F. Y. Yang, *Phys. Rev. B.* **88**, 100406(R) (2013).
22. N. Nagaosa, J. Sinova, S. Onoda, A. H. MacDonald, and N. P. Ong, *Rev. Mod. Phys.* **82**, 1539 (2010).
23. C. Pfleiderer and A. Rosch, *Nature* **465**, 880 (2010).
24. J. Sinova, J. Wunderlich, and T. Jungwirth, *Handbook of Spin Transpransport and Magnetism*, ed. E.Y. Tsymbal and I. Zutic. (CRC Press, New York) (2011).
25. B. Lebech, J. Bernhard, and T. Freltoft, *J. Phys. Condens. Matter* **1**, 6105 (1989).

Figure Captions

Figure 1: Semi-log 2θ-ω XRD scans of 100, 65, and 36 nm FeGe films epitaxially grown on Si(111).

Figure 2: (a) STEM image of a 100 nm FeGe thin film viewed along the FeGe <110> axis near the interface with Si(111). A 1.2-1.5 nm interfacial transition region is observed between the diamond structure of Si to the B20 structure of FeGe. (b) A high resolution STEM image of the FeGe film reveals the B20 ordering of Fe and Ge atoms. (c) Schematic of the cubic lattice and the <110> projection of the B20 structure.

Figure 3: (a) Out-of-plane magnetic hysteresis loop of the 36 nm FeGe film at 5 K. (b) Total Hall resistivity (ρ_{xy}) of the 36 nm FeGe film with a coercivity of 2400 Oe (T = 5 K) reveals a dominant topological Hall effect, which has a path opposite of the expected anomalous Hall effect. (c) The topological Hall resistivity (ρ_{TH}) hysteresis loops for the 36, 65, and 100 nm FeGe films at 5 K show a clear skyrmion phase, which exhibit substantial remanent values at H = 0, demonstrating robust skyrmion formation in the absence of magnetic field. (d) Semi-log plot of the temperature dependence of the maximum ρ_{TH} for the three samples. (e) The *Squareness* of the topological Hall resistivity, $\rho_{TH}(H = 0)/\rho_{TH}(\max)$, for the three FeGe films between 5 and 275 K, reflecting the stability of skyrmions at zero field.

Figure 4: Contour plots of ρ_{TH} for the (a), (b) 100 nm, (c), (d) 65 nm, and (e)-(h) 36 nm FeGe films. The plots on the left have the field sweeping from +7 to -7 T and the plots on the right have the field sweeping in the opposite direction. A zoom-in view of the 36 nm film in (g) and (h) highlights that nonzero topological Hall resistivity exists at zero field for all temperatures, particularly at low temperatures with substantial remanence at H = 0.

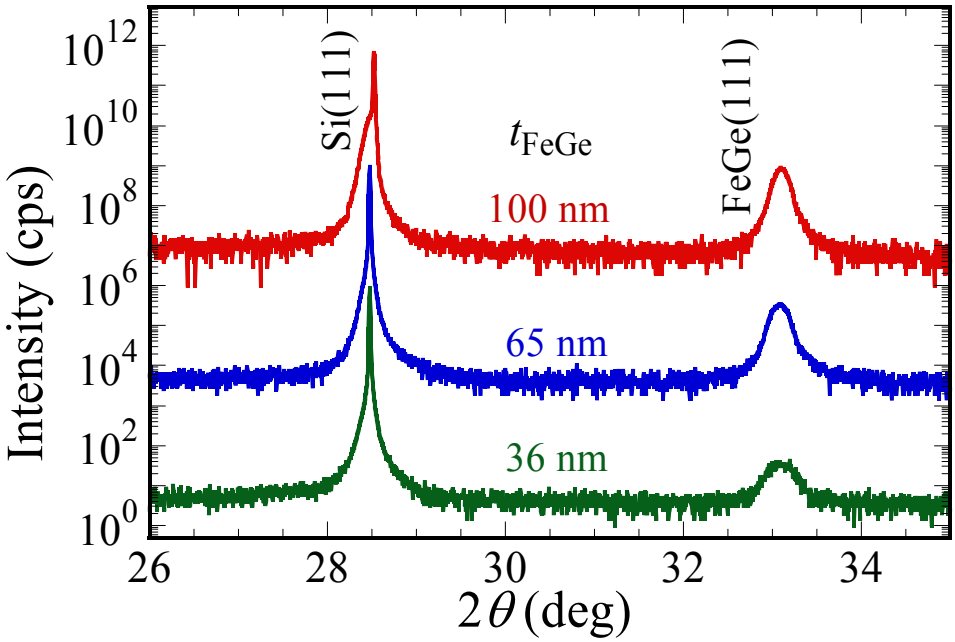
Intensity (cps)
10^{12}
10^{10}
10^{8}
10^{6}
10^{4}
10^{2}
10^{0}
Si(111)
FeGe(111)
t_{FeGe}
100 nm
65 nm
36 nm
26
28
30
32
34
2θ (deg)

Fig. 1

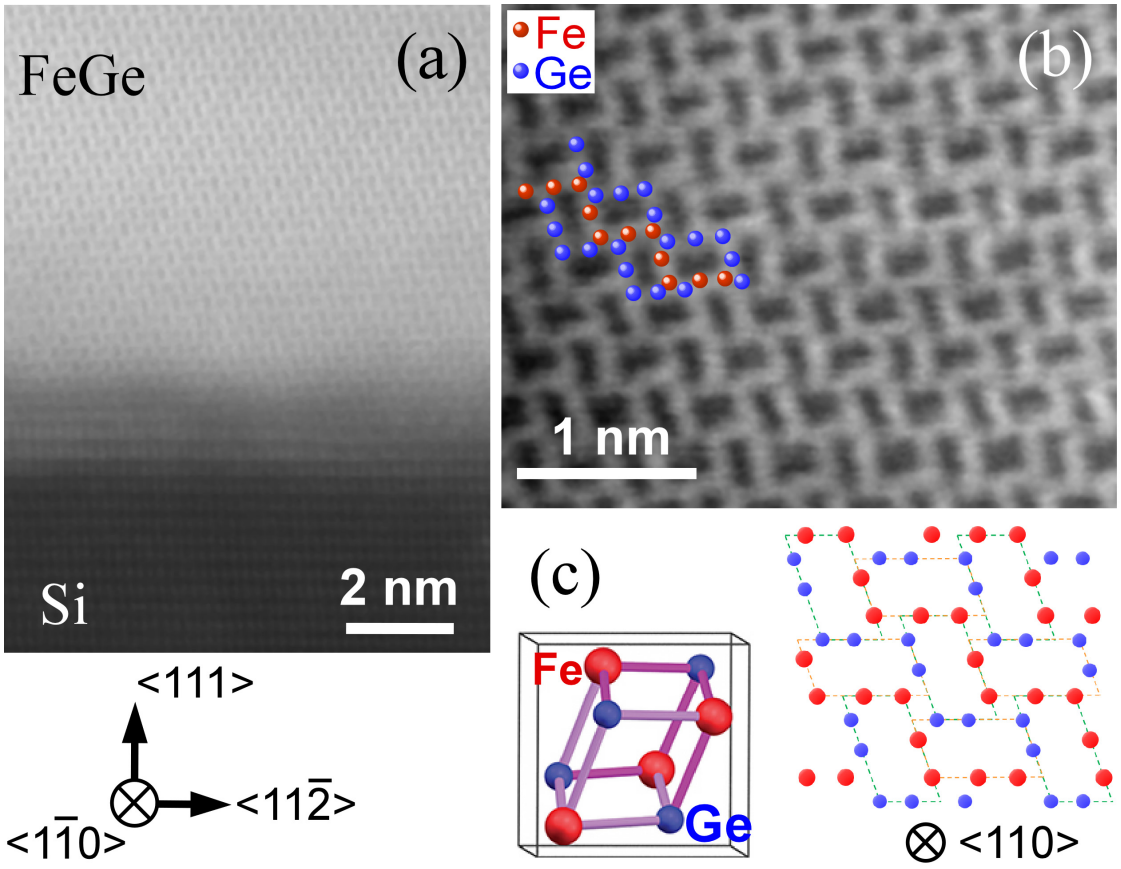

Fig. 2

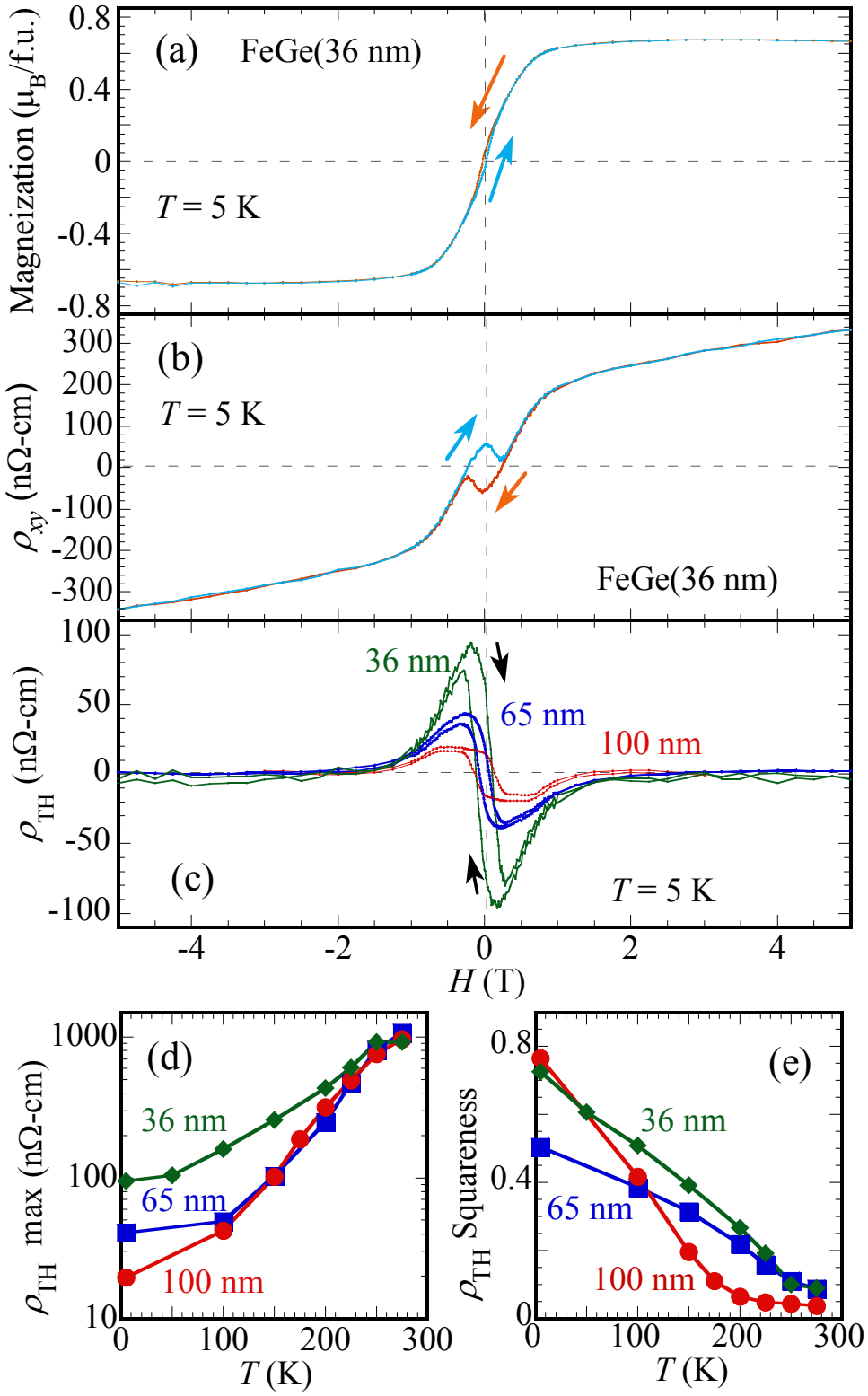
(a) FeGe(36 nm)
T = 5 K
Magneization (μB/f.u.)
0.8
0.4
0
-0.4
-0.8
(b)
T = 5 K
FeGe(36 nm)
ρxy (nΩ-cm)
300
200
100
0
-100
-200
-300
(c)
T = 5 K
36 nm
65 nm
100 nm
ρTH (nΩ-cm)
100
50
0
-50
-100
-4
-2
0
2
4
H (T)
(d)
36 nm
65 nm
100 nm
ρTH max (nΩ-cm)
1000
100
10
0
100
200
300
T (K)
(e)
36 nm
65 nm
100 nm
ρTH Squareness
0.8
0.4
0
0
100
200
300
T (K)

Fig. 3

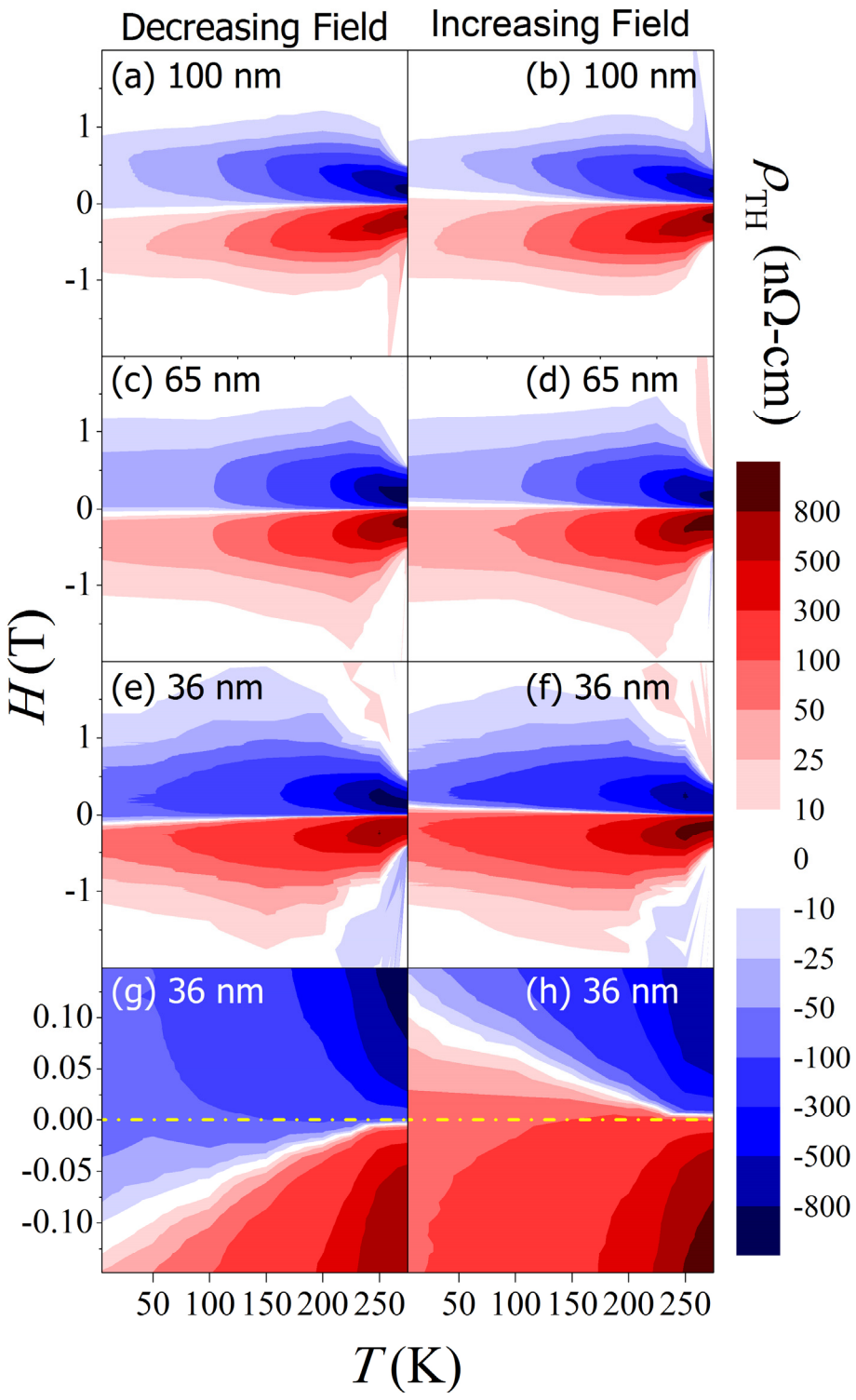
Decreasing Field
Increasing Field
(a) 100 nm
(b) 100 nm
(c) 65 nm
(d) 65 nm
(e) 36 nm
(f) 36 nm
(g) 36 nm
(h) 36 nm
H (T)
T (K)
ρTH (nΩ-cm)
800
500
300
100
50
25
10
0
-10
-25
-50
-100
-300
-500
-800

Fig. 4